Received: 14 August 2022 | Revised: 22 November 2022 | Accepted: 22 November 2022

DOI: 10.1111/jace.18919

Journal of the American Ceramic Society

RESEARCH ARTICLE

Enhanced electrical properties of Cr_2O_3 addition NBT-based high-temperature piezoelectric ceramics

Yanyan Zhang[1,2] | **Ruihong Liang**[1] | **Zhiyong Zhou**[1]

[1]Shanghai Institute of Ceramics, Key Laboratory of Inorganic Functional Materials and Devices, Chinese Academy of Sciences, Shanghai, People's Republic of China

[2]College of Materials Science and Opto-Electronic Technology, University of Chinese Academy of Sciences, Beijing, People's Republic of China

Correspondence
Zhiyong Zhou, Shanghai Institute of Ceramics, Key Laboratory of Inorganic Functional Materials and Devices, Chinese Academy of Sciences, 588 Heshuo Road, Jiading District, Shanghai 201899, People's Republic of China.
Email: zyzhou@mail.sic.ac.cn

Funding information
National Natural Science Foundation of China, Grant/Award Number: 51932010

Abstract

Owing to industrial and technological developments, there has been an increasing demand for piezoelectric ceramics that can function at temperatures of 500°C or higher. $Na_{0.5}Bi_{4.5}Ti_4O_{15}$ (NBT) with its high Curie temperature (T_C) of 650°C is a typical bismuth layer–structured ferroelectric. However, its relatively low piezoelectric coefficient ($d_{33} \sim 16$ pC/N) hinders its potential application at high temperatures. In this study, compositions of $Ca_{0.05}(Na_{0.5}Bi_{0.5})_{0.95}Bi_4Ti_4O_{15}$ with different additions of Cr_2O_3 (CNBT–Cr100x) were designed based on previous studies on Ca^{2+}-doped NBT piezoceramics, and the effects of the addition on the structural and electrical properties were investigated. The d_{33} value of CNBT–Cr20 was as high as 29 pC/N, almost twice higher than that of pure NBT ceramics. This increase was investigated in depth using X-ray diffraction refinement and piezoelectric force microscopy in terms of intrinsic and extrinsic contributions. The P_s values of CNBT and CNBT–Cr20 were almost equal. The density of the domain walls of CNBT–Cr20 was significantly higher than that of CNBT, indicating that the increase of d_{33} of CNBT–Cr20 is mainly due to the increase in the extrinsic contribution. The CNBT–Cr20 ceramic exhibited excellent properties with a high T_C of 655°C, a high d_{33} of 29 pC/N, and a resistivity high than 10^6 Ω cm at 500°C, demonstrating its potential for applications at high temperatures such as 500°C.

KEYWORDS

BLSFs, Cr2O3, Na0.5Bi4.5Ti4O15, piezoelectric coefficient

1 | INTRODUCTION

Piezoelectric materials with electromechanical coupling characteristics are essential smart materials for preparing various sensors, actuators, and transducers, which are widely used in several fields, such as aerospace, electronics, medical, biological, and energy.[1] Owing to substantial industrial development, piezoelectric devices are required to operate in a wide range of temperatures. For instance, in the automotive electronics industry, to improve the efficiency and reliability of internal combustion engines, piezoelectric sensors are used to measure the temperature of the engine before ignition, when they are operating in an environment of high-temperature thermal cycles (>500°C).[2] The Curie temperature (T_C) and piezoelectric coefficient (d_{33}) of high-temperature piezoelectric ceramics, which are key components of high-temperature sensors, are the most critical evaluation factors for their proper operation. T_C not only determines the depolarization temperature and service temperature of piezoelectric ceramics but also ensures that ceramics are not susceptible to aging effects in a significantly lower

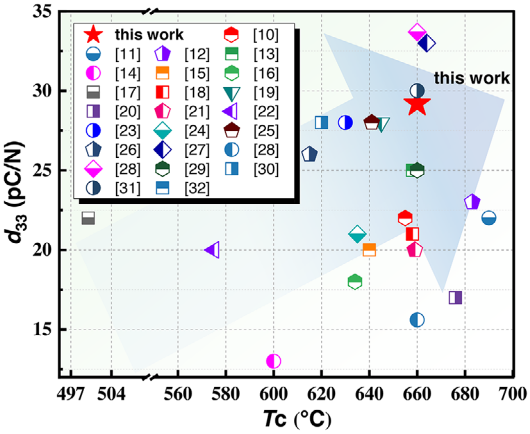

FIGURE 1 Summary of d_{33} and T_C of some $Na_{0.5}Bi_{4.5}Ti_4O_{15}$-based modification works so far

temperature range. Perovskite-structured piezoelectric ceramics, among which lead zirconate titanate ($Pb(Zr,Ti)O_3$, PZT) is a representative example, are the most successful commercially available piezoelectric materials, the $T_C < 400°C$ and service temperature (≤300°C) of which are relatively low; hence, they cannot be used at higher temperatures. Presently, there is an urgent need to investigate high-temperature piezoelectric ceramics that can be applied in environments with temperatures of 500°C or higher.

Bismuth layer–structured ferroelectrics (BLSFs) with the general formula $(Bi_2O_2)^{2+}(A_{n-1}B_nO_{3n+3})^{2-}$ are an important category of lead-free ferroelectrics and piezoelectric materials that have potential applications in high-temperature sensors because of their high T_C and large spontaneous polarization (P_s).[3] Their structure is a symbiosis of $(A_{n-1}B_nO_{3n+3})^{2-}$ units and $(Bi_2O_2)^{2+}$ slabs along the vertical direction. However, the P_s of BLSFs is significantly anisotropic and can only be oriented along the *a*-axis, limiting the polarization flip of the defective dipoles to the *a*–*b* plane, which naturally results in a low piezoelectric coefficient. A high piezoelectric coefficient enables the piezoelectric material to exhibit a large mechanical response or large electrical response when an external electric field or force field is applied, which directly determines the sensitivity of high-temperature sensors.[4] Among all the BLSFs used for high-temperature piezoelectric sensors at 500°C, $Na_{0.5}Bi_{4.5}Ti_4O_{15}$ (NBT) has a relatively high d_{33} (~16 pC/N) and a suitable T_C (~650°C). However, the d_{33} of NBT ceramics is not sufficiently high to use it as the key component of piezoelectric sensors in most applications, necessitating further improvement.

In perovskite materials such as PZT, amphoteric dopants with both soft and hard characteristics, such as MnO_2, CeO_2, and Cr_2O_3, yield satisfactory results in improving their piezoelectric properties. It has been demonstrated that $0.75BiFeO_3$–$0.25BaTiO_3$ modified with Mn can achieve a d_{33} of 110 pC/N.[5] The addition of 0.3 wt% Cr_2O_3 to a $Pb(Zn_{1/3}Nb_{2/3})_{0.20}(Zr_{0.50}Ti_{0.50})_{0.80}O_3$ system resulted in a more stable tetragonal phase relative to the rhombohedral phase, increasing the d_{33} from 420 to 490 pC/N.[6] Yan et al. investigated the effect of Cr_2O_3 addition on the crystal structure and properties of $PbZr_xTi_y(Mg_{1/3}Nb_{2/3})_{1-x-y}O_3$ and reported an increase in d_{33} by 50 pC/N.[7] Notably, recent studies have reported that Cr_2O_3 has similarly improved the piezoelectric properties of BLSF piezoelectric materials. For instance, among modifications with MnO_2, CeO_2, and Cr_2O_3, that with Cr_2O_3 provided the best improvement in the d_{33} and thermal stability of $SrBi_4Ti_4O_{15}$.[8] In addition, Cr_2O_3 addition had positive effects on the piezoelectric properties of W^{6+}-doped $Bi_4Ti_3O_{12}$ and $CaBi_2Nb_2O_9$, with an increase in the d_{33} values to 28[9] and 15 pC/N[3], respectively. The addition of moderate amounts of Cr_2O_3 also effectively improved the fracture strength of the BIT component due to the induction of large grains or low fracture toughness. The substitution of Ti^{4+} by Cr^{3+} affects the tilt of the oxygen octahedron and the electrical properties of the material by creating oxygen vacancies in the oxygen octahedron.

In our previous study, we investigated the effect of the Ca^{2+} substitution of $(Na_{0.5}Bi_{0.5})^{2+}$ at site A on the structure and electrical properties of NBT and observed that the composition $(Na_{0.5}Bi_{0.5})_{0.95}Ca_{0.05}Bi_4Ti_4O_{15}$ (CNBT) had superior piezoelectric properties.[10] In this study, Cr_2O_3 was added to obtain a $(Na_{0.5}Bi_{0.5})_{0.95}Ca_{0.05}Bi_4Ti_4O_{15} + 0.2\%\ Cr_2O_3$ material, and as expected, an excellent piezoelectric coefficient d_{33} of 29 pC/N and a high T_C of 655°C were achieved. This newly designed NBT-based piezoceramic exhibits outstanding performance compared to most NBT-modified materials as shown in Figure 1.[10–34] The effect of Cr_2O_3 addition on the structure and dielectric, ferroelectric, and piezoelectric properties of the CNBT ceramics was further explored.

2 | MATERIALS AND METHODS

Ceramics with compositions of $Ca_{0.05}(Na_{0.5}Bi_{0.5})_{0.95}Bi_4Ti_4O_{15} + x$ wt% Cr_2O_3 ($x = 0$, 0.1, 0.2, and 0.3, abbreviated as CNBT–Cr100*x*: CNBT, CNBT–Cr10, CNBT–Cr20, and CNBT–Cr30, respectively) were prepared using a conventional solid-state reaction. According to the composition design, the raw materials and their purities were Bi_2O_3 (99.9%), Na_2CO_3 (99.8%), TiO_2 (99.62%), $CaCO_3$ (99%), and Cr_2O_3 (99%). The raw materials were ball-milled with alcohol and agate balls for 4 h according to the stoichiometric compositions for thorough mixing. Thereafter, the mixture was dried at 80°C for approximately 3 h. It was subsequently calcined at 850°C for 2 h to allow it to

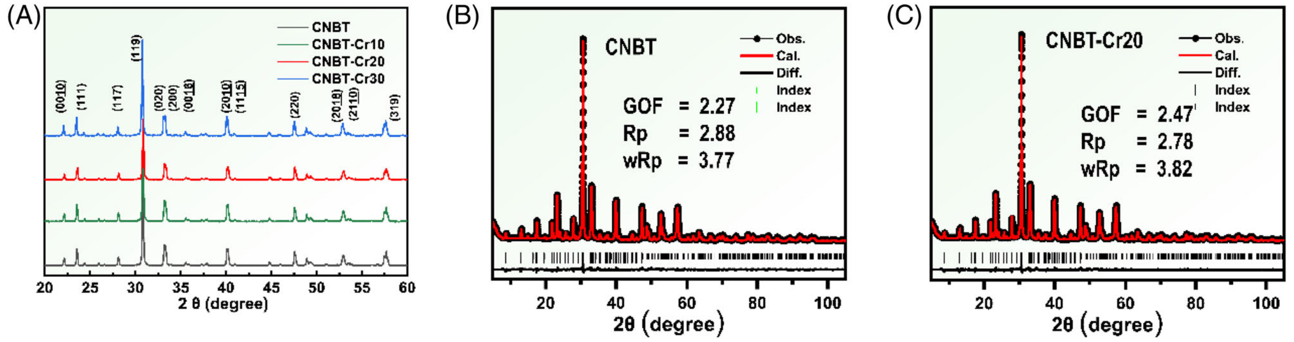

FIGURE 2 (A) X-ray diffraction (XRD) patterns of CNBT–Cr100*x* ceramics; Rietveld refinement for (B) CNBT and (C) CNBT–Cr20

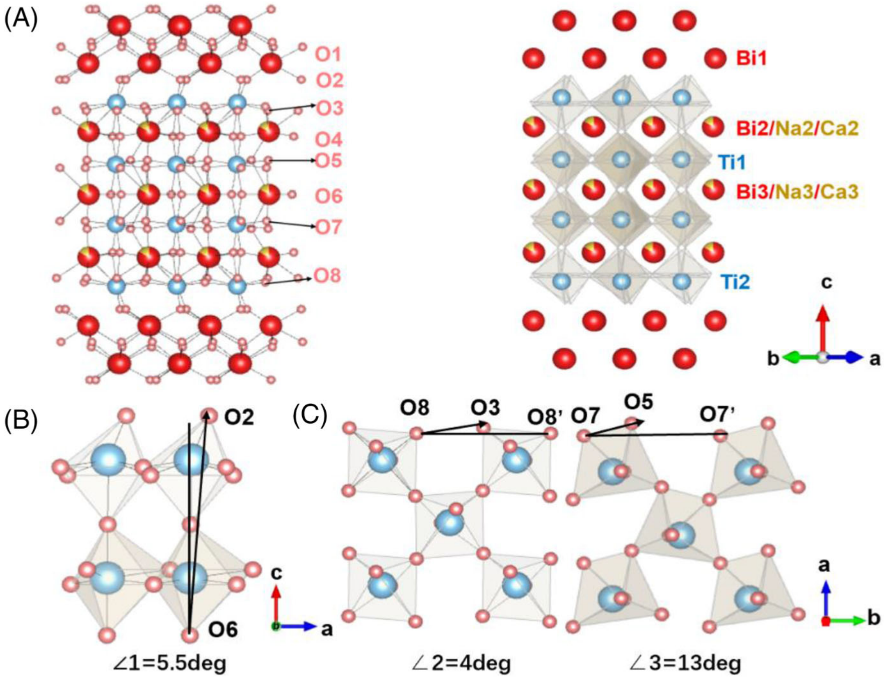

FIGURE 3 (A) Unit cell morphology and atomic positions of CNBT–Cr100*x*; degree of tilt (B) and rotation (C) of pseudo-perovskite of CNBT–Cr20

TABLE 1 Tilt and rotation of TiO_6 of CNBT

	∠1	∠2	∠3
CNBT	5.2°	4°	12.9°

sufficiently react to form new species. The new substance and Cr_2O_3 were ground with alcohol for 6 h to reduce the particle size while mixing Cr_2O_3 uniformly with NBT. The powder with small particles was combined with 6% PVA as a binder to form larger particles, which were pressed into disks with a diameter of 13 mm. The green bodies were sintered at 1150°C for 2 h and thereafter processed into ceramic sheets of a uniform thickness of 0.5 mm.

To study the internal structure of the ceramics more carefully, one of the sides of the ceramic pieces was polished, and the crystal structure of the ceramic blocks was measured through X-ray diffraction (XRD, Rigaku RAX-10, Tokyo, Japan, $\lambda = 1.54056$ Å) with Cu K_α radiation. Refined initial XRD data were obtained using the ceramic powder. The sizing and scanning times for the two steps were 0.02° for 8 min and 0.003° for 2 h, respectively. The microstructures of the ceramic pieces were examined using a benchtop scanning electron microscope (Hitachi, Tokyo, Japan). A piezoelectric reaction force microscope (MFP-3D, Asylum Research, USA) was used to characterize the structural domains. The force constant of the piezoelectric force microscopy (PFM) conductive cantilever beam was 2.8 N/m, and the resonance frequency was 75 Hz. To test the electrical properties of the CNBT–Cr100*x* ceramics, they were covered with Pt electrodes and sintered at 850°C for half an hour. Subsequently, the dielectric constant and loss versus temperature were measured using an impedance material analyzer (Model DMS-1000, Partulab, China) and an instrument (Model E4990A; Keysight, USA). The magnitudes of the remanent polarization and the coercive field were obtained using an electrical analyzer (TF Analyzer 2000, aixACCT, Aachen, Germany) at 1 Hz and 180°C. The piezoelectric coefficient was measured at room temperature using a quasi-static ZJ-3AM d_{33} meter (Institute of Acoustics, Chinese Academy of Sciences, China). The variation of DC resistivity with temperature was measured using an HRMS-900 conductivity measurement device (Partulab, Wuhan, China).

3 | RESULTS AND DISCUSSION

Figure 2 shows the XRD patterns of the polished piezoceramics of the CNBT–Cr100*x* compositions, reflecting their crystal structures. The positions of all the major peaks are observed to be in good agreement with the PDF card (#52-1640), indicating that the crystal phase is not affected by the addition of Cr_2O_3. The strongest peak of the CNBT–Cr100*x* ceramics is for the (119) reflection, which is consistent with the fact that the main peak of the BLSFs ceramics is at (112*m* + 1).[26] Rietveld refinement analysis was performed for the CNBT and CNBT–Cr20 powders using the *A*21*am* space group, and the calculated results agreed well with the experimental data (GOF, Rp, and wRp were less than 5).

As shown in Figure 3, the effect of Cr_2O_3 addition on the crystal structure of CNBT–Cr100*x* was explored in depth using Vesta. In BLSFs, the degree of distortion of the pseudo-perovskite layer is commonly used to indicate the lattice distortion of the ceramics.[10,27] One unit cell of the CNBT–Cr100*x* ceramic contains eight types of oxygen atoms and two types of pseudo-perovskite. Here, the degree of tilt is expressed by angle 1 ($\angle 1$) between the vertex oxygen atoms O2 and O6 of the two [TiO_6] octahedra and the *c*-axis. The degree of rotation of the octahedron is indicated by angle 2 ($\angle 2$) between O3, O8, and the *b* axis and angle 3 ($\angle 3$) between O5, O7, and the *b* axis. A comparison of $\angle 1$, $\angle 2$, and $\angle 3$ of CNBT and CNBT–Cr20 indicates that the addition Cr_2O_3 has little effect, as illustrated in Figure 3B,C and Table 1, mainly because of the small amount of Cr_2O_3 entering the lattice and the similar radii of Cr^{3+} (0.615 Å) and Ti^{4+} (0.605 Å).

The microscopic morphology of the ceramic grains of CNBT–Cr100*x* is shown in Figure 4. The CNBT–Cr100*x* series of ceramics has a unique morphology of irregular platelet-like grains similar to other BLSFs, which leads to the generation of partial pores.[15] The relative denseness of the ceramics can be observed from the cross-sectional images illustrated in Figure 4(a2)–(d2). The grain sizes of CNBT–Cr20 and CNBT–Cr30 are larger than those of CNBT. According to the sintering theory, the grain surface and grain boundary energies are the main driving forces for sintering and grain growth, which are closely related to the migration of ions. Therefore, the addition of Cr_2O_3 affects the activation energy of ion migration in CNBT–Cr100*x*, resulting in grain growth.

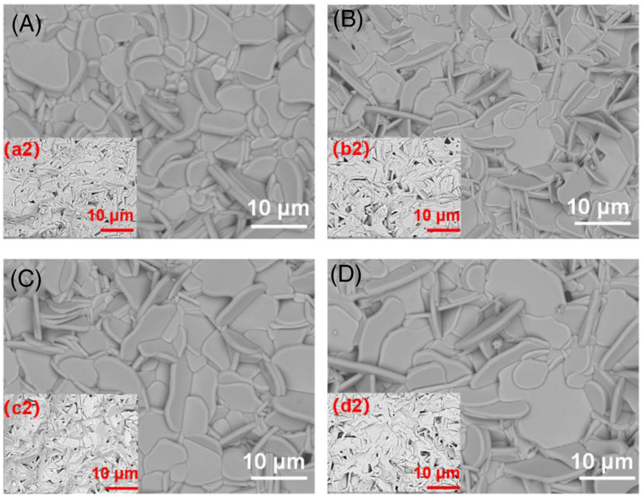

FIGURE 4 SEM images of natural surfaces of (A) CNBT, (B) CNBT–Cr10, (C) CNBT–Cr20, and (D) CNBT–Cr30 ceramics; SEM images of cross sections of (a2) CNBT, (b2) CNBT–Cr10, (c2) CNBT–Cr20, and (d2) CNBT–Cr30 ceramics

The dielectric constant and loss versus temperature curves of the unpoled CNBT–Cr100*x* are shown in Figure 5. When Ca^{2+} replaces $(Na_{0.5}Bi_{0.5})^{2+}$ at site A, the T_C of CNBT–Cr100*x* ceramics is slightly higher than that of NBT (approximately 650°C). The modification of Cr_2O_3 has no significant effect on the T_C of CNBT–Cr100*x* ceramics, which remains at approximately 655°C, indicating that it is directly related to the insignificant lattice distortion illustrated in Figure 3. The dielectric peaks of CNBT–Cr100*x* are sharp and the dielectric constant varies smoothly with temperature, demonstrating the stability of the dielectric properties. Furthermore, influenced by the positive effect of Ca^{2+}, the dielectric loss of CNBT–Cr100*x* is less than that of NBT.[10] As the concentration of Cr_2O_3 increases, the dielectric loss of CNBT–Cr100*x* gradually increases, which is related to the increase in the concentration of defects.

The ferroelectric properties of the CNBT–Cr100*x* ceramics are illustrated in Figure 6, which were all measured at 1 Hz and 180°C. The remanent polarization (P_r) of the CNBT–Cr100*x* ceramics increases significantly with the addition of Cr_2O_3. However, with the addition of Cr_2O_3, the hysteresis loop gradually becomes unsaturated, and the saturation hysteresis loop of CNBT–Cr30 cannot be measured even if the temperature or frequency is changed. The relatively small P_r is caused by the pinning of the domain walls (DWs).[35] The charge defects (mainly oxygen

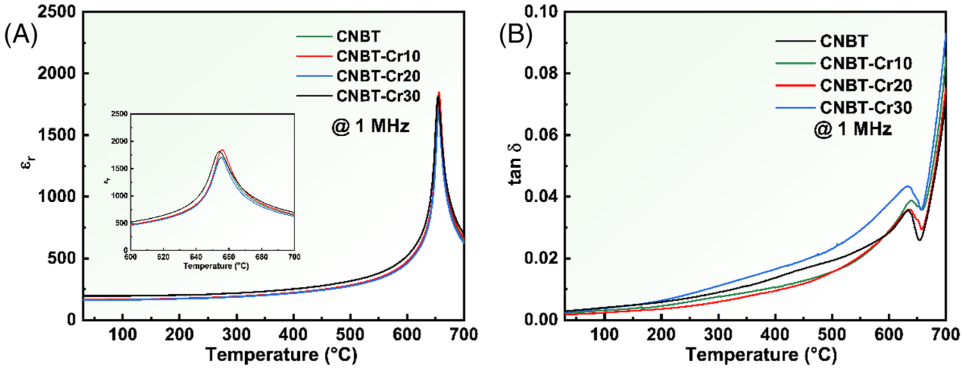

FIGURE 5 Dielectric properties of CNBT–Cr100*x*: dielectric constant (A) and dielectric loss (B) versus temperature at 1 MHz

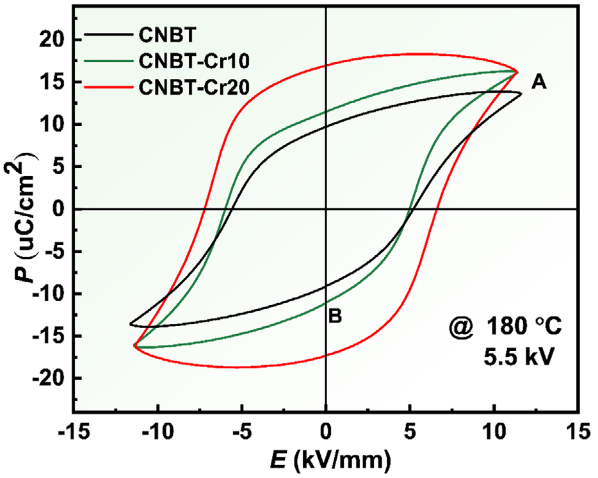

FIGURE 6 Ferroelectric properties of CNBT–Cr100*x* ceramics at 180°C: *P*–*E* loops of CNBT, CNBT–Cr10, and CNBT–Cr20

vacancies) are absorbed by the DWs, which are pinned when the concentration of defects in their vicinity reaches a critical value. Therefore, a high DW density or a small number of defects may enhance the polarization properties of the ceramics. It has been proven that the slope of the right-hand side of the *P*–*E* curve with respect to the coercive field (E_c) is related to the mobility of the ferroelectric domains.[36] The slope of the curve between points A and B in Figure 5 increases significantly with the addition of Cr_2O_3, indicating that the mobility of the ferroelectric domains of CNBT–Cr100*x* becomes easier with respect to that of pure CNBT. However, the leakage currents of CNBT–Cr20 and CNBT–Cr30 increase significantly owing to the carrier concentration.

To further analyze the variation in the concentration of oxygen vacancies and the electrical properties of the materials, the variations in the DC resistivity (ρ) and activation energy (E_a) of the CNBT–Cr100*x* ceramics with temperature were investigated, and the results are shown in Figure 7. With the addition of Cr_2O_3, the resistivity decreases significantly in the low-temperature region and gradually approaches that of the high-temperature region. E_a can be determined using the Arrhenius formula, and the specific values are shown in Figure 7B. The fluctuations in the E_a values at different temperature intervals illustrate the different conduction mechanisms of CNBT–Cr100*x* in the high- and low-temperature regions. The conduction mechanism of pure NBT ceramics is a mixture of p-type and ion-type conductions, where the concentration of carriers is related to the concentration of $V_O^{\bullet\bullet}$.[27] To balance the carrier charges, the bismuth vacancies in the BLSFs caused by Bi volatilization generate several oxygen vacancies. The holes generated by the oxygen vacancies trapping oxygen are involved in conduction as carriers, as expressed in the following equations:

$$2Bi_{Bi}^{\times} + 3O_O^{\times} \rightarrow 2V_{Bi}''' + 3V_O^{\bullet\bullet} + Bi_2O_3 \quad (1)$$

$$V_O^{\bullet\bullet} + 0.5O_2 \rightarrow 2h^{\cdot} + O_O^{\times} \quad (2)$$

At lower temperatures, E_a is almost equal to the value of the secondary ionization of oxygen vacancies, indicating that the conduction mechanism is dominated by hole conduction related to oxygen vacancies.[27] At higher temperatures, E_a is almost equal to half the E_g of BLSFs, proving that ionic conduction dominates the conduction mechanism in this temperature range. The change in the conduction mechanism is consistent with the change in resistivity. At lower temperature, more oxygen vacancies are generated owing to the substitution of Ti^{4+} at the B site by Cr^{3+}, which reduces the resistivity of CNBT–Cr100*x*, as expressed in the following equation:

$$Cr_2O_3 \xrightarrow{Ti} 3V_O^{\bullet\bullet} + 2Cr_{Ti} + 4e \quad (3)$$

As the temperature increases, the contribution of intrinsic carriers to the conductivity increases, causing the conductivities of CNBT–Cr100*x* to become very close to each other when it equals or even exceeds the

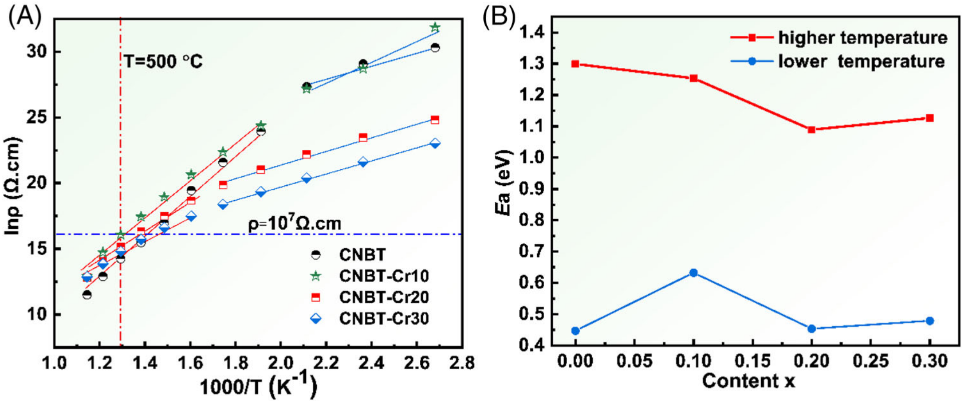

FIGURE 7 (A) DC resistivity and (B) activation energy of CNBT–Cr100*x* ceramics changes with temperature

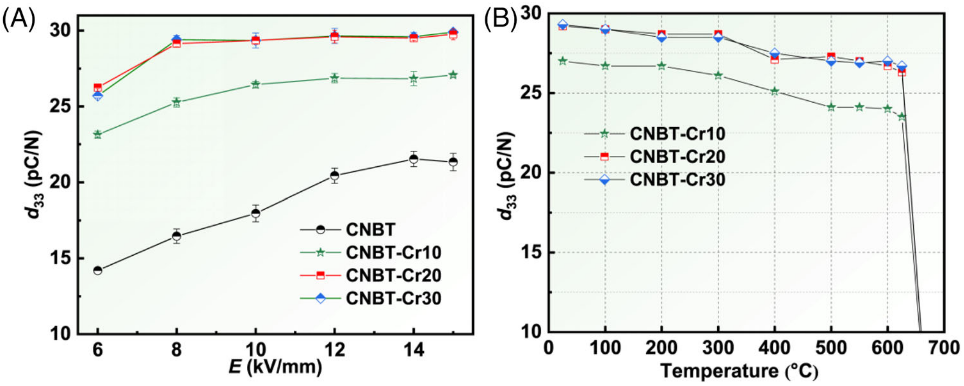

FIGURE 8 Variation of d_{33} of CNBT–100*x* with polarization voltage from 6 to 15 kV/mm. (A) Variation of d33 of CNBT-Cr100x with polarization voltage from 6 kV/mm to 15 kV/mm; (B) The thermal stability of d33 of CNBT-Cr100x from 25°C to 660°C

effect of addition. The ρ–T curve gradually converges in the high-temperature region. At 500°C, the resistivity of CNBT–Cr100*x* is greater than 10^6 Ω cm. The lower conductivity at high temperatures can reduce the charge drift and ensure the practical application of piezoelectric ceramics at high temperatures. In addition, it can be seen from Figure 7 that the transition temperature from hole conduction to ion conduction gradually shifts to the high-temperature region as the concentration of Cr_2O_3 increases.

The piezoelectric coefficient of the CNBT–Cr100*x* ceramics versus the applied voltage during polarization is shown in Figure 8. The samples were polarized under electric fields of 6, 8, 10, 12, and 14 kV/mm for 10 min. CNBT–Cr20 and CNBT–Cr30 exhibited a high piezoelectric coefficient (approximately 29 pC/N), significantly higher than the d_{33} of 22 pC/N for CNBT and close to twice that of NBT ceramics (16 pC/N). In addition, the domains of CNBT–Cr20 and CNBT–Cr30 essentially switch at an electric field of 8 kV/mm, with little change in d_{33} when the electric field is increased further. In comparison with the pure CNBT ceramics, CNBT–Cr20 and CNBT–Cr30 complete domain switching at a high electric field of 14 kV/mm, indicating that their domain switching is much easier. The good thermal stabilities of d_{33} of CNBT–Cr100*x* are obtained from Figure 8B, with a variation of less than 10% from room temperature to 500°C.

The spontaneous polarization values of the CNBT and CNBT–Cr20 ceramics were determined to identify the reasons for the increased piezoelectric coefficient, and the results are shown in Figure 9. The piezoelectric response of ferroelectric materials includes internal and external contributions, where the internal response is the contribution of atomic displacements at the unit cell level. In BLSFs, the spontaneous polarization (P_s) originates from the displacement of atoms along the *a*-axis during the ferroelectric phase transition. Larger lattice distortions help increase the spontaneous polarization and improve the piezoelectric properties of ceramics.[37] P_s can be calculated using the Shimakawa model as follows[38]:

$$P_s = \sum_i (m_i \times \Delta x_i \times Q_i e) / V,$$

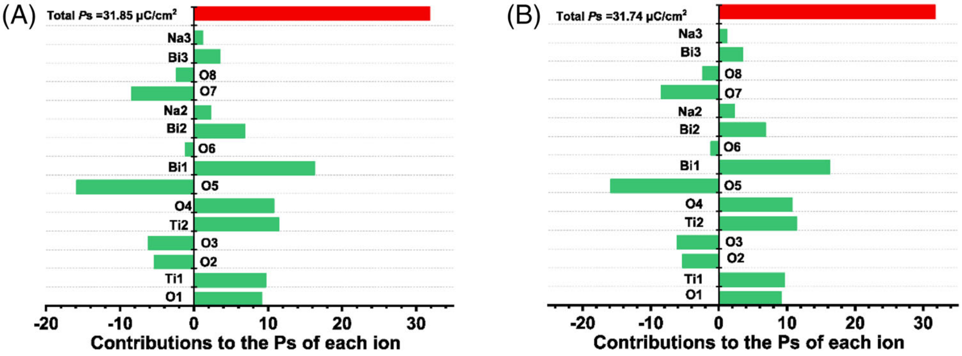

FIGURE 9 Contribution of each atom to spontaneous polarization for (A) CNBT and (B) CNBT–Cr20

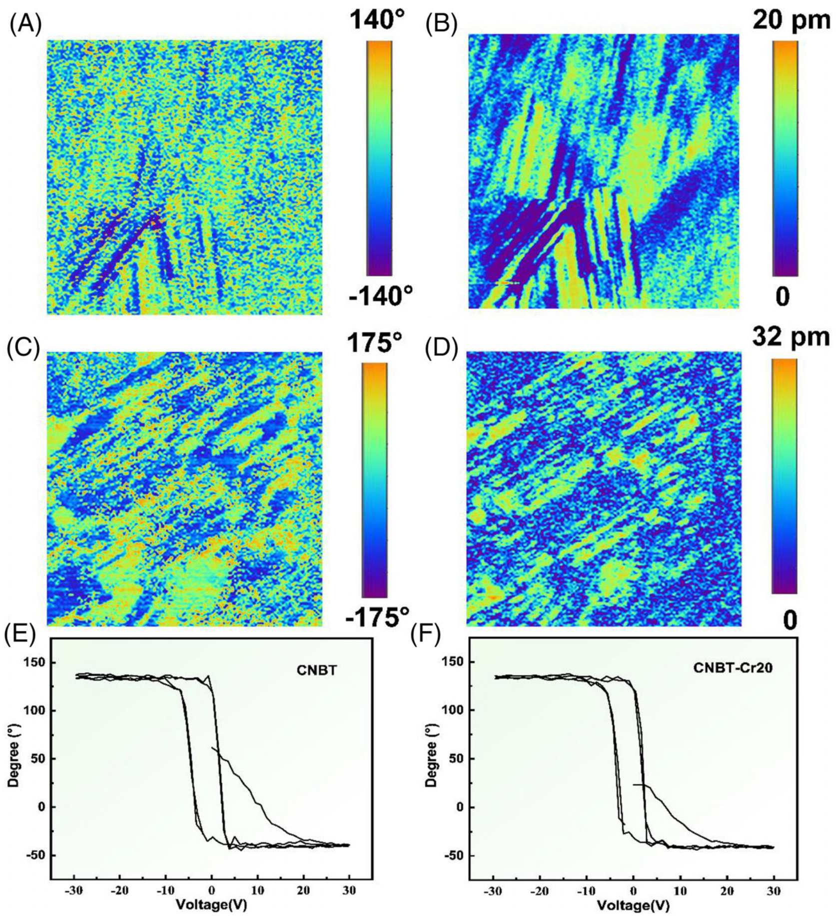

FIGURE 10 Piezoresponse force microscopy (PFM) in 3 μm × 3 μm: out-of-plane PFM phase of (A) CNBT and (C) CNBT–Cr20; images of (B) CNBT and (D) CNBT–Cr20 ceramics; phase hysteresis loops of (E) CNBT and (F) CNBT–Cr20

where m_i denotes the lattice multiplicity, Δx_i is the displacement of each atom along the a-axis, $Q_i e$ is the charge of the ith component ion, and V is the unit cell volume. It can be seen from Figure 9A,B that even if all of the 0.2 wt% Cr_2O_3 enters the lattice of CNBT–Cr100x, the P_s values of CNBT and CNBT–Cr20 do not change significantly, indicating that the increase in the d_{33} of CNBT–Cr20 has no effect on the intrinsic contribution. The total P_s is mainly contributed by the displacement of the A-site ions and ions in the TiO_6 octahedron.

PFM is a powerful technique for studying ferroelectric phenomena, such as ferroelectric domain inversion, fatigue and storage mechanisms, and phase transitions of ferroelectric materials.[39–41] The external contribution to the piezoelectric response of ferroelectric materials is related to domains and DWs. The d_{33} value of ferroelectric ceramics is determined by the macroscopic polarization arrangement induced by the external electric field, which results from the alignment of the dipole along the direction of the applied electric field. The spontaneous polarization of most BLSFs is along the *a*-axis; therefore, 90° and 180° ferroelectric DWs are more likely to be present in the CNBT–Cr100*x* ceramics.[42] The phase hysteresis loops illustrated in Figure 10E,F indicate that, there are 180° DWs in CNBT–Cr100*x*. As shown in Figure 10A,C, the phases of the CNBT and CNBT–Cr20 ceramics have a stripe-like morphology similar to the domains of other BLSFs.[33] The DWs density of the CNBT–Cr20 ceramics is significantly higher than that of CNBT, which is favorable for improving d_{33}. The magnitude of the piezoelectric response is reflected in the images illustrated in Figure 10B,D, where that for CNBT–Cr20 is greater than that for CNBT, corresponding to the actual relative magnitude of the piezoelectric coefficient.

4 | CONCLUSIONS

In this study, a series of CNBT–Cr100*x* ceramics with the crystal structures and microscopic morphologies consistent with classical morphologies of BLSFs were through conventional solid-state synthesis. Cr_2O_3 entered the lattice of the B site and replaced Ti^{4+}, thus increasing the electrical conductivity at low temperatures. At high temperatures, the conduction mechanism changed from electron to ion conduction. The resistivity of CNBT–Cr100*x* gradually converged at high temperatures and was higher than 10^6 Ω cm at 500°C, confirming the suitability of the ceramic for application at high temperatures. CNBT–Cr100*x* ceramics have a high T_C around 655°C and low dielectric loss. The CNBT–Cr20 ceramics exhibited a higher piezoelectric coefficient of 29 pC/N and were more easily fully polarized at low electric fields. The reasons for the increase in d_{33} in CNBT–Cr20 were explored in terms of the intrinsic and extrinsic contributions. The P_s values of CNBT (31.85 $\mu C/cm^2$) and CNBT–Cr20 (31.76 $\mu C/cm^2$) were almost equal. The density of the DWs of CNBT–Cr20 was higher than that of CNBT, which made the domain switching of CNBT–Cr20 easier. The high T_C (655°C), high d_{33} (29 pC/N), and high resistivity (>10^6 Ω cm, @500°C) of the CNBT–Cr20 piezoelectric ceramics indicate their potential stability and suitability for application at 500°C.

ACKNOWLEDGMENT

This work was supported by the National Natural Science Foundation of China (Grant No. 51932010).

ORCID

Yanyan Zhang https://orcid.org/0000-0001-5395-3831
Ruihong Liang https://orcid.org/0000-0002-0761-0915
Zhiyong Zhou https://orcid.org/0000-0002-1546-7741

REFERENCES

1. Thong HC, Li Z, Lu JT, Li CBW, Liu YX, Sun Q, et al. Domain engineering in bulk ferroelectric ceramics via mesoscopic chemical inhomogeneity. Adv Sci. 2022;9:202200998.
2. Stevenson T, Martin DG, Cowin PI, Blumfield A, Bell AJ, Comyn TP, et al. Piezoelectric materials for high temperature transducers and actuators. J Mater Sci Mater Electron. 2015;26(12):9256–67.
3. Chen ZN, Sheng LS, Li XD, Zheng P, Bai WF, Li L, et al. Enhanced piezoelectric properties and electrical resistivity in W/Cr co-doped $CaBi_2Nb_2O_9$ high-temperature piezoelectric ceramics. Ceram Int. 2019;45(5):6004–11.
4. Yan YK, Geng LWD, Zhu LF, Leng HY, Li X, Liu H, et al. Ultrahigh piezoelectric performance through synergistic compositional and microstructural engineering. Adv Sci. 2022;9(14):202105715.
5. Chen JG, Tong BB, Lin JY, Gao XY, Cheng JR, Zhang S. Tailoring the chemical heterogeneity of Mn-modified $0.75BiFeO_3$-$0.25BaTiO_3$ ceramics for piezoelectric sensor applications. J Eur Ceram Soc. 2022;42(9):3857–64.
6. Hou YD, Lu PX, Zhu MK, Song XM, Tang JL, Wang B, et al. Effect of Cr_2O_3 addition on the structure and electrical properties of $Pb((Zn_{1/3}Nb_{2/3})_{0.20}(Zr_{0.50}Ti_{0.50})_{0.80})O_3$ ceramics. Mater Sci Eng B—Adv. 2005;116(1):104–8.
7. He LX, Gao M, Li CE, Zhu WM, Yan HX. Effects of Cr_2O_3 addition on the piezoelectric properties and microstructure of $PbZr_xTi_y(Mg_{1/3}Nb_{2/3})_{1-x-y}O_3$ ceramics. J Eur Ceram Soc. 2001;21(6):703–9.
8. Wang SZ, Zhou HJ, Wu DW, Li L, Chen Y. Effects of oxide additives on the phase structures and electrical properties of $SrBi_4Ti_4O_{15}$ high-temperature piezoelectric ceramics. Materials. 2021;14(20):6227.
9. Chen Y, Xie SX, Wang HM, Chen Q, Wang QY, Zhu J, et al. Dielectric abnormality and ferroelectric asymmetry in W/Cr co-doped $Bi_4Ti_3O_{12}$ ceramics based on the effect of defect dipoles. J Alloys Compd. 2017;696:746–53.
10. Zhang YY, Ke XC, Zhao KY, Zhou ZY, Liang RH. Ca^{2+} doping effects on the structural and electrical properties of $Na_{0.5}Bi_{4.5}Ti_4O_{15}$ piezoceramics. Ceram Int. 2022;48:31265–72.
11. Zuo YD, Fang ZY, Fan DM, Liu KH, Niu H, Wang H, et al. Interrelation between lattice structures and polarization in high Curie temperature piezoelectric $Na_{0.5}Bi_{4.46}Ce_{0.04}Ti_{4-x}Co_xO_y$ ceramics. Ceram Int. 2022;48(7):9297–303.
12. Chen Y, Du YK, Fan DM, Niu HY, Zuo YD, Hu L, et al. Study on the polarization enhancement mechanism and electrical properties of high temperature bismuth layered $K_xNa_{0.5-x}Bi_{4.46}Ce_{0.04}Ti_4O_{15+y}$ ceramics. Ceram Int. 2021;47(20):29023–9.
13. Wu WF, Han YX, Huang X, Du J, Bai W, Wen F, et al. Electrical properties of a Cr_2O_3-modified $Na_{0.5}Bi_{4.5}Ti_4O_{15}$-$Na_{0.5}Bi_{0.5}TiO_3$ composite ceramic. J Aust Ceram Soc. 2021;57(2):321–6.
14. Yao MW, Yu GB, Zhu CM, Wang LG, Zeng PY. Phase transition induced morphotropic phase boundary behavior and the electric properties in strontium modulated $Bi_{4.5}Na_{0.5}Ti_4O_{15}$ lead-free ceramics. Ceram Int. 2021;47(16):22889–99.
15. Qin L, Jiang CB, Liu KH, Chen Y, Du YK, Zuo Y, et al. Structural and electric properties of Ce-doped $Na_{0.5}Bi_{4.5}Ti_4O_{15}$ piezoceramics with high Curie temperatures. J Am Ceram Soc. 2020;103(8):4083–9.

16. Chen Y, Zhang CC, Qin L, Jiang CB, Liu KH, Ma C, et al. Enhanced dielectric and piezoelectric properties in $Na_{0.5}Bi_{4.5}Ti_4O_{15}$ ceramics with Pr-doping. Ceram Int. 2018;44(15):18264–70.
17. Jiang YL, Jiang XP, Chen C, Chen YJ, Jiang X, Tu N, et al. Structural and electrical properties of La^{3+}-doped $Na_{0.5}Bi_{4.5}Ti_{4.5}O_{15}$-$Bi_4Ti_3O_{12}$ inter-growth high temperature piezoceramics. Ceram Int. 2017;43(8):6446–52.
18. Yao ZR, Chu RQ, Xu ZJ, Hao JG, Li W, Li G. Thermal stability and enhanced electrical properties of Er^{3+}-modified $Na_{0.5}Bi_{4.5}Ti_4O_{15}$ lead-free piezoelectric ceramics. RSC Adv. 2016;6(97):94870–5.
19. Abah R, Gai ZG, Zhan SQ, Zhao ML. The effect of B-site (W/Nb) co-substituting on the electrical properties of sodium bismuth titanate high temperature piezoceramics. J Alloys Compd. 2016;664:1–4.
20. Jiang XG, Jiang XP, Chen C, Tu N, Chen YJ, Zhang BC. Photoluminescence, structural, and electrical properties of erbium-doped $Na_{0.5}Bi_{4.5}Ti_4O_{15}$ ferroelectric ceramics. J Am Ceram Soc. 2016;99(4):1332–9.
21. Li N, Ma WB, Zang XR, Wang YY, Guo JD, Zhao HD, et al. Effect of K content to lead-free $SrBi_4Ti_4O_{15}$-$(Na_{0.5}Bi_{0.5})Bi_4Ti_4O_{15}$ piezoelectric ceramics. J Mater Sci Mater Electron. 2016;27(12):12473–8.
22. Meng XY, Ma WB, Chen TK, Wang MY, Guo YX. The piezoelectric properties of $SrBi_4Ti_4O_{15}$-$Na_{0.5}Bi_{4.5}Ti_4O_{15}$ solid solution. J Electron Mater. 2015;11(5):902–5.
23. Jiang XP, Fu XL, Chen C, Na TU, Xu MZ, Li XH, et al. High performance Aurivillius type $Na_{0.5}Bi_{4.5}Ti_4O_{15}$ piezoelectric ceramics with neodymium and cerium modification. J Adv Ceram. 2015;4(1):7.
24. Du H, Xiang S. Dielectric and piezoelectric properties of barium-modified Aurivillius-type $Na_{0.5}Bi_{4.5}Ti_4O_{15}$. J Phys Chem Solids. 2011;72(11):1279–83.
25. Gai ZG, Feng YY, Wang JF, Wu H. The effect of (Li,Ce) doping in Aurivillius phase material $Na_{0.5}Bi_{4.5}Ti_4O_{15}$. Adv Mater Res. 2011;146–147:89–92.
26. Feng YY, Zhang Y, Gai ZG, Hu P, Zhou YF, Wang LiH, et al. The high-performance of cerium doped sodium bismuth titanate aurivillirs phase material. Adv Mater Res. 2011;284–286:1389–92.
27. Xi JW, Xing J, Chen H, Zhang FF, Chen Q, Zhang W, et al. Crystal structure and electrical properties of Li/Mn co-doped NBT-based Aurivillius-type ceramics. J Alloys Compd. 2021;868:159216.
28. Takenaka, S, Sakata K, Toda K. Piezoelectric properties of bismuth layer-structured ferroelectric $Na_{0.5}Bi_{4.5}Ti_4O_{15}$ ceramic. Jpn J Appl Phys. 1985;24:730.
29. Wang CM, Wang JF. High performance Aurivillius phase sodium-potassium bismuth titanate lead-free piezoelectric ceramics with lithium and cerium modification. Appl Phys Lett. 2006;89:202905.
30. Wang CM, Wang JF, Gai ZG. Enhancement of dielectric and piezoelectric properties of $M_{0.5}Bi_{4.5}Ti_4O_{15}$ (M = Na, K, Li) ceramics by Ce doping. Scr Mater. 2007;57:789–92.
31. Wang CM, Wang JF, Zhang SJ. Electromechanical properties of A-site (LiCe)-modified sodium bismuth titanate ($Na_{0.5}Bi_{4.5}Ti_4O_{15}$) piezoelectric ceramics at elevated temperature. J Appl Phys. 2009;105:094110.
32. Wang CM, Zhao L, Wang JF, Zhang SJ, Shrout TR. Enhanced piezoelectric properties of sodium bismuth titanate ($Na_{0.5}Bi_{4.5}Ti_4O_{15}$) ceramics with B-site cobalt modification. Phys Status Solidi. 2009;3:7–9.
33. Zhao TL, Guo ZL, Wang CM. The effects of Na/K ratio on the electrical properties of sodium-potassium bismuth titanate $Na_{0.5}Bi_{4.5}Ti_4O_{15}$-$K_{0.5}Bi_{4.5}Ti_4O_{15}$. J Am Ceram Soc. 2012;95:1062–7.
34. Wang CM, Zhao L, Liu Y, Withers RL, Zhang S, Wang Q. The temperature-dependent piezoelectric and electromechanical properties of cobalt-modified sodium bismuth titanate. Ceram Int. 2016;42:4268–73
35. Scott JF, Dawber M. Oxygen-vacancy ordering as a fatigue mechanism in perovskite ferroelectrics. Appl Phys Lett. 2000;76(25):3801–3.
36. Xie XC, Zhou ZY, Gao BT, Zhou ZY, Liang RH, Dong XL. Ion-pair engineering-induced high piezoelectricity in $Bi_4Ti_3O_{12}$-based high-temperature piezoceramics. Acs Appl Mater Inter. 2022;14(12):14321–30.
37. Yi ZG, Wang Y, Li YX, Yin QR. Ferroelectricity in intergrowth Bi_3TiNbO_9-$Bi_4Ti_3O_{12}$ ceramics. J Appl Phys. 2006;99(11):114101.
38. Shimakawa Y, Kubo Y, Nakagawa Y, Kamiyama T, Asano H, Izumi F. Crystal structures and ferroelectric properties of $SrBi_2Ta_2O_9$ and $Sr_{0.8}Bi_{2.2}Ta_2O_9$. Appl Phys Lett. 1999;74(13):1904–6.
39. Eitel R, Randall CA. Octahedral tilt-suppression of ferroelectric domain wall dynamics and the associated piezoelectric activity in $Pb(Zr,Ti)O_3$. Phys Rev B. 2007;75(9):094106.
40. Anthoniappen J, Chang WS, Soh AK. Electric field induced nanoscale polarization switching and piezoresponse in Sm and Mn co-doped $BiFeO_3$ multiferroic ceramics by using piezoresponse force microscopy. Acta Mater. 2017;132:174–81.
41. Anthoniappen J, Chang WS, Ruiz FM. Electric field and temperature induced local polarization switching and piezoresponse in $Bi_{0.88}Sm_{0.12}FeO_3$ ceramics for nanoscale applications. J Alloys Compd. 2019;790:587–96
42. Xie XC, Zhou ZY, Liang RH, Dong XL. Superior piezoelectricity in bismuth titanate-based lead-free high-temperature piezoceramics via domain engineering. Adv Electron Mater. 2022;8(7):2101266.

How to cite this article: Zhang Y, Liang R, Zhou Z. Enhanced electrical properties of Cr_2O_3 addition NBT-based high-temperature piezoelectric ceramics. J Am Ceram Soc. 2023;106:2357–2365. https://doi.org/10.1111/jace.18919